Supporting Information

Sirajuddin et al. 10.1073/pnas.0902858106

SI Text

Construction of pFM835 (*CDC11-His$_6$* and *MBP-CDC12* in pMalcHis Vector) and pFM846 (*CDC11-His$_6$* and *MBP-cdc12H155A* in pMalcHis Vector) for Bicistronic Expression. For the bicistronic plasmid pFM835, *CDC11* (primer CDC11-POLY14J and primer CDC11-POLYCI13C, template pFM581) and *CDC12* (primer CDC12-N1 and primer POLYCI4a, template pFM338) were amplified. The PCR products were digested with BamHI and SacI for *CDC12* or with SacI and SalI for *CDC11*, and both fragments were introduced between BamHI and SalI of pMalcHis (1) as a 3-fragment ligation. Bicistronic plasmid pFM846 was constructed like pFM835, with the exception of using pFM651 as a template for *cdc12H155A* amplification.

Construction of pFM847 (*MBP-CDC3* and *CDC10-His$_6$* in pMalcHis-kan) and pFM848 (*MBP-cdc3H262A* and *CDC10-His$_6$* in pMalcHis-kan) for Bicistronic Expression. For the bicistronic plasmid pFM847, *CDC3* (primer CDC3bicN and primer CDC3bicC, template pFM337) and *CDC10* (primer CDC10bicN and primer CDC10bicC, template pFM580) were amplified. The PCR products were digested with BamHI and SacI for *CDC3* or with SacI and SalI for *CDC10*, and both fragments were introduced between BamHI and SalI of pFM455 (1) as a 3-fragment ligation. Bicistronic plasmid pFM848 was constructed like pFM835, with the exception of using pFM582 as a template for *cdc3H262A* amplification.

Expression and Purification of Binary Complexes. For the bacterial expression of yeast binary complexes, corresponding plasmid was transformed in *E. coli* strain BL21 (DE3) Rosetta (Novagen). Strains transformed with plasmid pFM835 expressed Cdc11-His$_6$ and MBP-Cdc12, strains with plasmids pFM846 expressed CDC11-His$_6$ and MBP-cdc12H155A, strains with pFM847 expressed MBP-CDC3 and CDC10-His$_6$, and strains with pFM848 expressed MBP-CDC3H262A and CDC10-His$_6$. The cells were grown on Terrific Broth (300 mL), supplemented with ampicillin or kanamycin and chloramphenicol, at 37 °C and induced at an optical density of OD_{600} = 0.6 via the addition of 0.5 mM Isopropyl β-D-1-thiogalactopyranoside. After 8 h at 37 °C, cells were harvested by centrifugation and resuspended in isolation buffer. Isolation was performed as described previously (1), but using small Ni-NTA (1.5 mL) and amylose (0.8 mL) columns. Further steps after the amylose column were omitted. The final products were analyzed by SDS-polyacrylamid electrophoresis.

Purification of SEPT2 Protein. Different constructs of SEPT2 WT and mutant proteins were expressed and purified as GST-fused proteins as described previously (2). The purified protein contained ≈50% GDP bound to it, and was exchanged to GppNHp by adding 1 U of shrimp alkaline phosphatase per mg protein and 3× excess of GppNHp. The exchange reaction was left overnight at 4 °C. The excess and unbound nucleotide was removed by size-exclusion chromatography.

Crystallization and Structure Determination. The initial crystallization condition was identified by semiautomatic nanoliter sitting-drop screening using commercial Qiagen/Nextal screening kits and a Mosquito pipetting station. The crystallization conditions were optimized to 1.4 M lithium acetate and 0.1 M Hepes buffer (pH 7.0) with hanging-drop vapor diffusion at 20 °C. The crystals were harvested and transferred to a cryoprotectant containing 20% glycerol along with mother liquor, which was then flash-frozen in liquid nitrogen. A data set to 2.9-Å resolution was collected at PXII SLS, Villigen, Switzerland. All data processing was done using the XDS software package (3).

The structure was solved by the molecular replacement program Molrep (4) using SEPT2-GDP coordinates (2QA5). Four molecules (2 dimers) were observed in an asymmetric unit. Electron density was noted for the gamma phosphate, magnesium ion, and several new regions in the protein, and the initial model was rebuilt using COOT (5). Refinement was done with Refmac5 (CCP4 suite) (6, 7), using the NCS and TLS body functions (see Table S1 for refinement statistics). The buried surface area was calculated using CNS (8) with a default probe radius of 1.4 Å. Figures were generated using Pymol (9).

Radioactive Charcoal Assay. GTP hydrolysis was measured using [γ^{32}P]GTP. First, 10 μM of SEPT2 WT and corresponding mutants were incubated in buffer at 30 °C. GTP hydrolysis was started by adding 150 μM GTP, including 30 nM [γ^{32}P]GTP (15 μCi). Aliquots of 10 μL were obtained at prespecified time points and mixed with 400 μL of charcoal solution (50 g·l^{-1} charcoal in 20 mM phosphoric acid) to stop the reaction. The charcoal was pelleted, and the amount of free ^{32}Pi in 180 μL of the supernatant was determined by scintillation counting. Relative counts were plotted against reaction time.

Nucleotide-Binding Experiments. SEPT2 WT and mutant protein were titrated against 500 nM 3′-*O*-(*N*-methyl)anthranoyl (mant)-nucleotides until saturation was reached. The mant fluorophore was excited at 360 nm, and emission was monitored at 450 nm (Fluoromax4; Horiba Jobin Yvon). The increased fluorescence after the addition of protein was integrated over at least 10 min, and the equilibrium dissociation constant, K_d, was calculated by fitting a quadratic function to the data. All experiments were performed at 20 °C in 50 mM Tris (pH 8.0), 150 mM NaCl, 5 mM $MgCl_2$, and 5 mM DTE buffer.

Viability of Yeast Septin Mutants. The yeast strains and plasmids used in this study are listed in Table S3. Yeast septin deletion strains were obtained from EUROSCARF (Frankfurt, Germany). Haploid deletion strains with a WT copy of the corresponding septin gene on centromeric plasmid pRS416 (10) were prepared by standard yeast genetic techniques (11). The yeast septin mutants were constructed in centromeric plasmid pRS415. These *CEN/LEU2* plasmids were then introduced in haploid deletion strains. Loss of *URA3* plasmid carrying an intact septin gene was assayed by platting serial dilutions of these strains on 5-FOA plates lacking leucine and grown at both permissive (28 °C) and nonpermissive (37 °C) temperatures.

1. Farkasovsky M, Herter P, Voss B, Wittinghofer A (2005) Nucelotide binding and filament assembly of recombinant yeast septin complexes. *Biol Chem* 386:643–656.
2. Sirajuddin M, et al. (2007) Structural insight into filament formation by mammalian septins. *Nature* 449:311–315.
2. Kabsch W (1993) Automatic processing of rotation diffraction data from crystals of initially unknown symmetry and cell constants. *J Appl Crystallogr* 26:795–800.
4. Vagin A, Teplyakov A (1997) MOLREP: An automated program for molecular replacement. *J Appl Crystallog* 30:1022–1025.
5. Emsley P, Cowtan K (2004) COOT: Model-building tools for molecular graphics. *Acta Crystallog D Biol Crystallog* 60:2126–2132.
6. The CCP4 suite: Programs for protein crystallography (1994) *Acta Crystallogr D Biol Crystallogr* 50:760–763.

7. Murshudov GN, Vagin AA, Dodson EJ (1997) Refinement of macromolecular structures by the maximum-likelihood method. *Acta Crystallogr D Biol Crystallog* 53:240–255
8. Brünger AT, et al. (1998) Crystallography & NMR system: A new software suite for macromolecular struture determination. *Acta Crystallogr D Biol Crystallogr* 54:905–921.
9. DeLano WL (2002) The PyMOL molecular grahics system. Available from http://www.pymol.org. Accessed March 3, 2009.
10. Sikorski RS, Hieter P (1989) A system of shuttle vectors and yeast host strains designed for efficienct manipulation of DNA in *Saccharomyces cerevisiae. Genetics* 122:19–27.
11. Ausubel FM, et al. (1987) *Current Protocols in Molecular Biology* (Wiley, New York), pp 2.10–2.11.

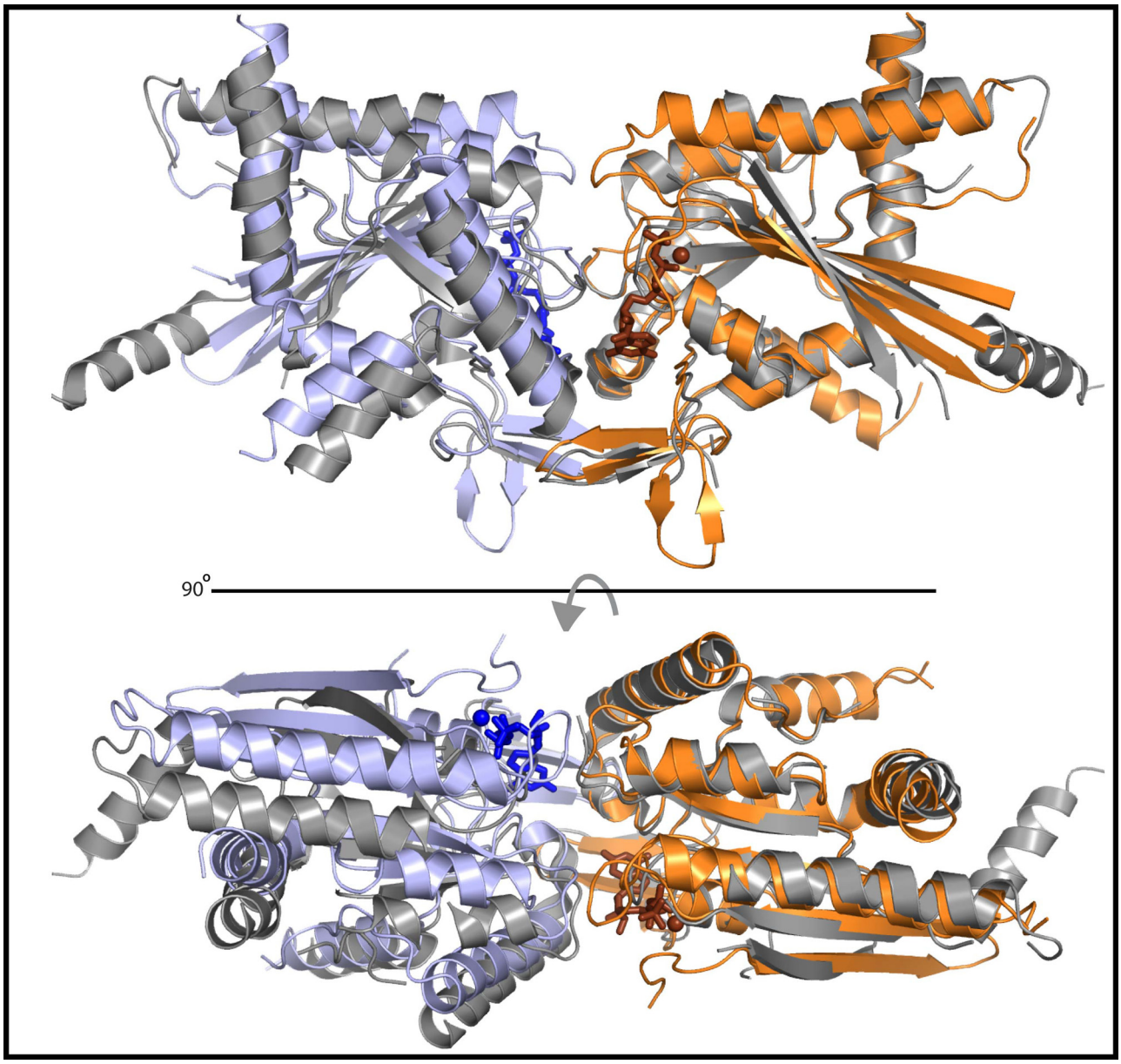

Fig. S1. Superimposition of SEPT2-GppNHp dimer (color) and SEPT2-GDP dimer (gray) showing the slight tilting of the GppNHp dimer.

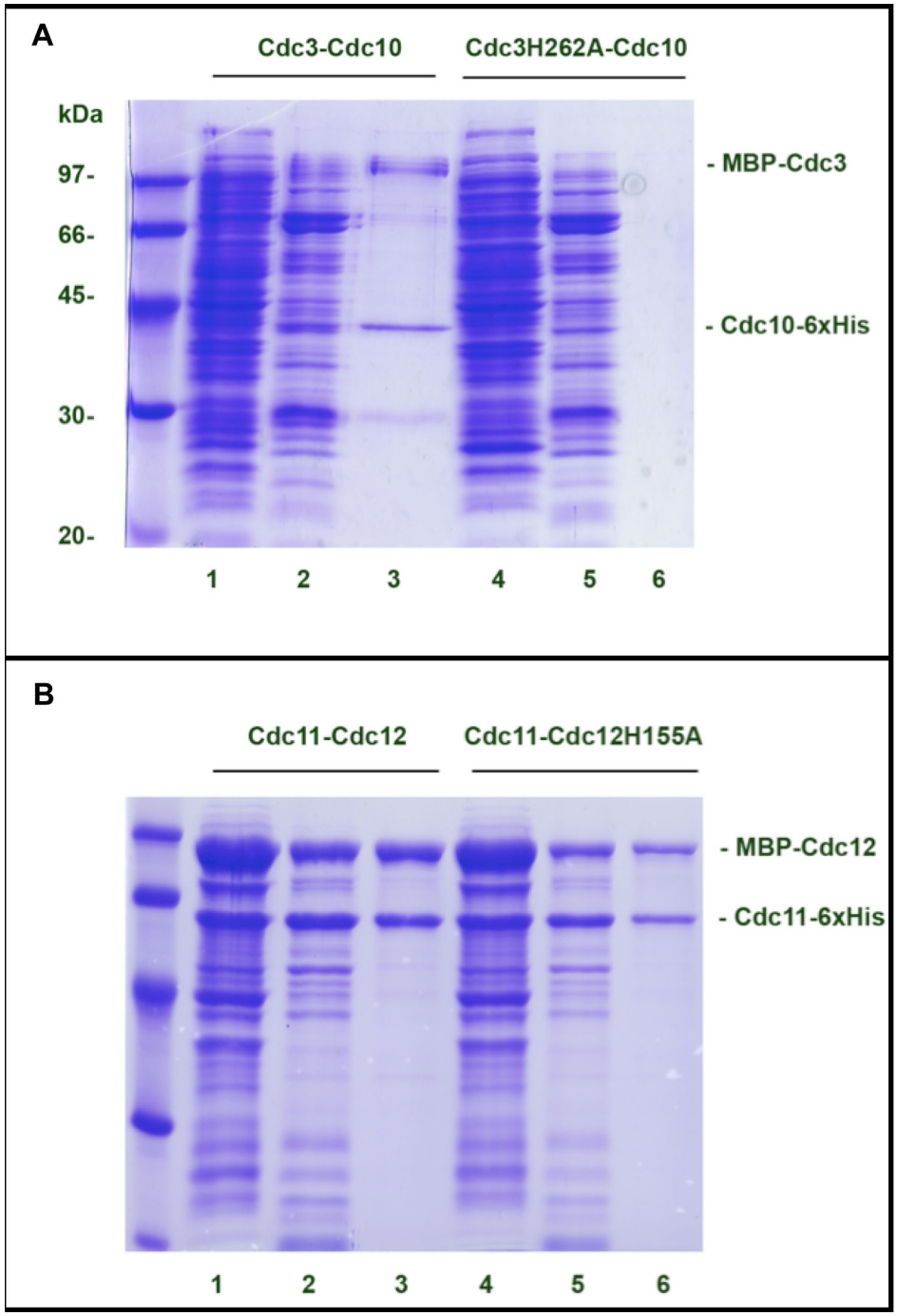

Fig. S2. Heterodimerzation studies of yeast binary septin complexes Cdc3–10 and Cdc11–12 WT and mutants. Lanes 1 and 4, protein extract; lanes 2 and 5, Ni-NTA elution; lanes 3 and 6, amylose elution.

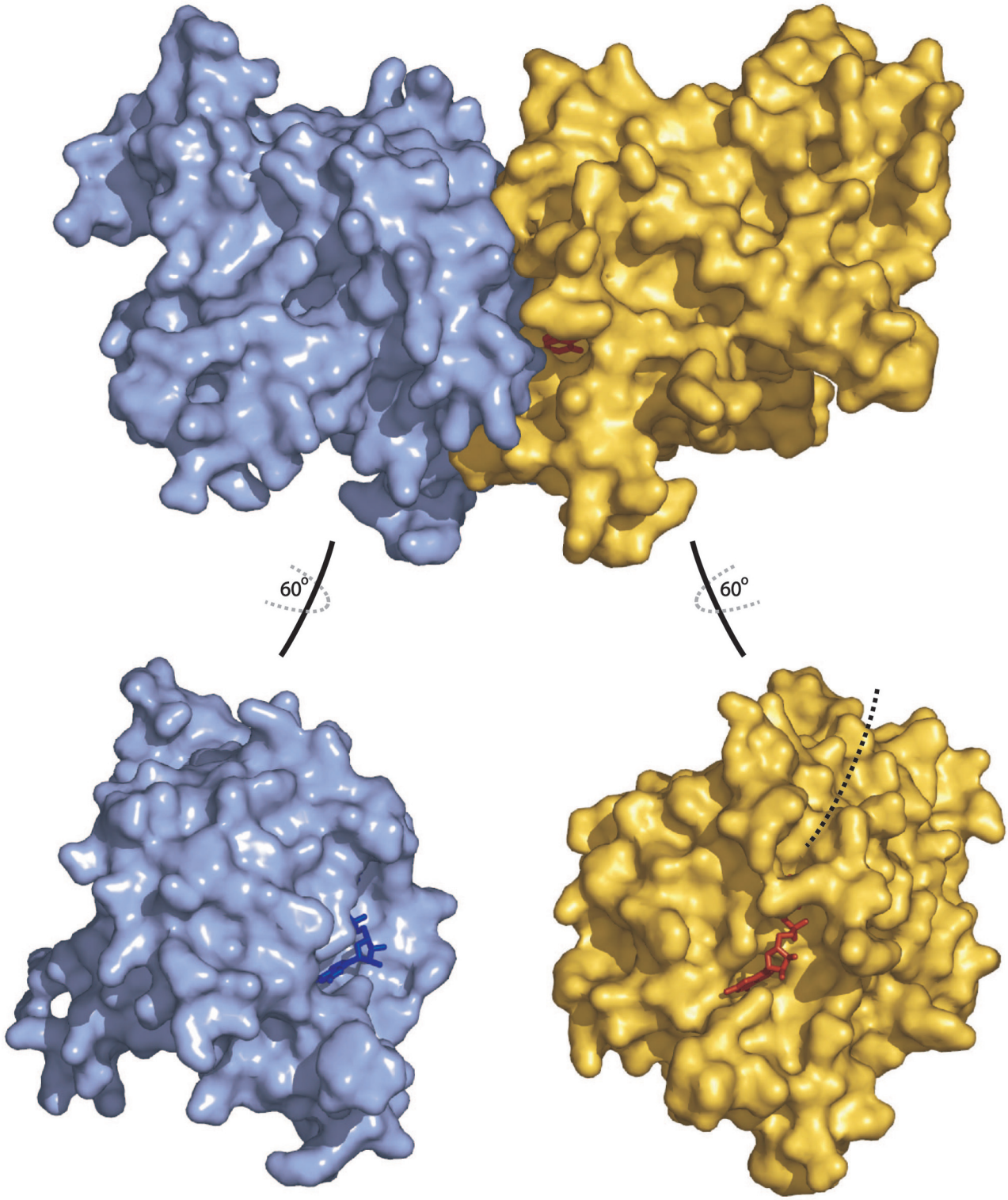

Fig. S3. Surface representation of SEPT2-GppNHP, with the nucleotide buried in the G interface. The dotted arrow indicates a small tunnel to the γ-phosphate.

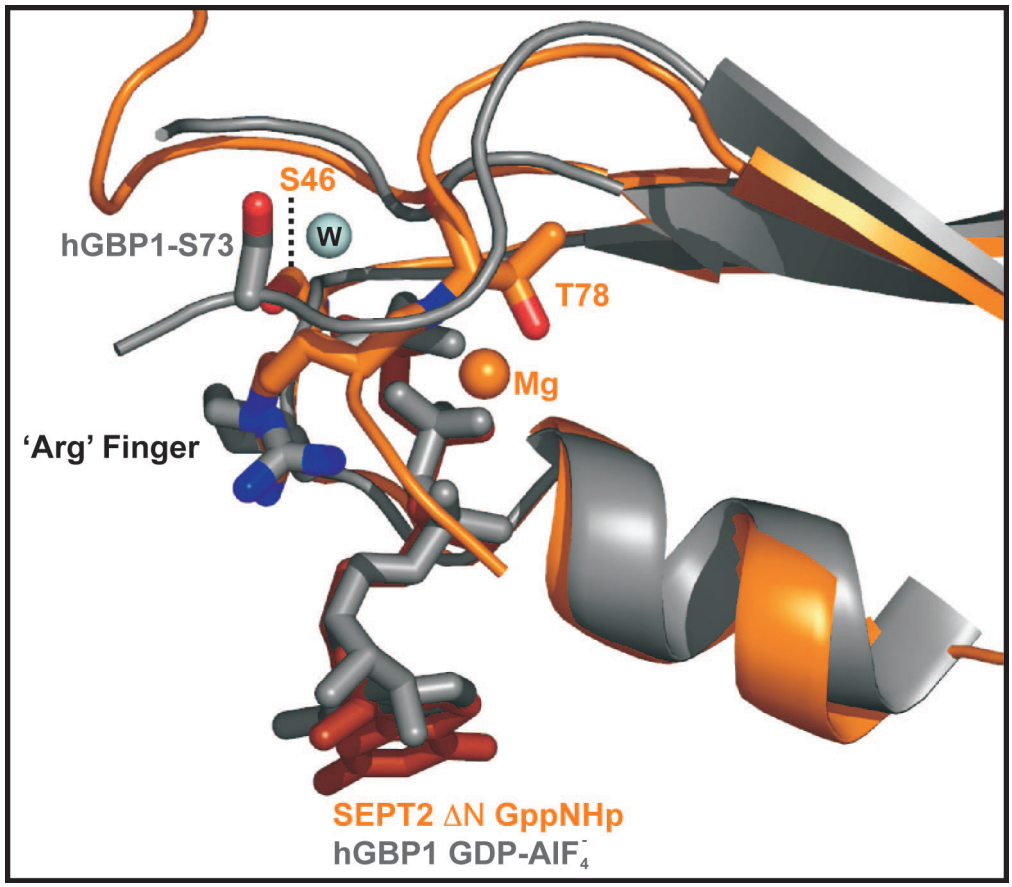

Fig. S4. Structural alignment of SEPT2-GppNHp (orange) with hGBP1-GDP-AlF4 (gray) (PDBID: 2B92). The serine and arginine occupy similar positions as seen in hGBP1.

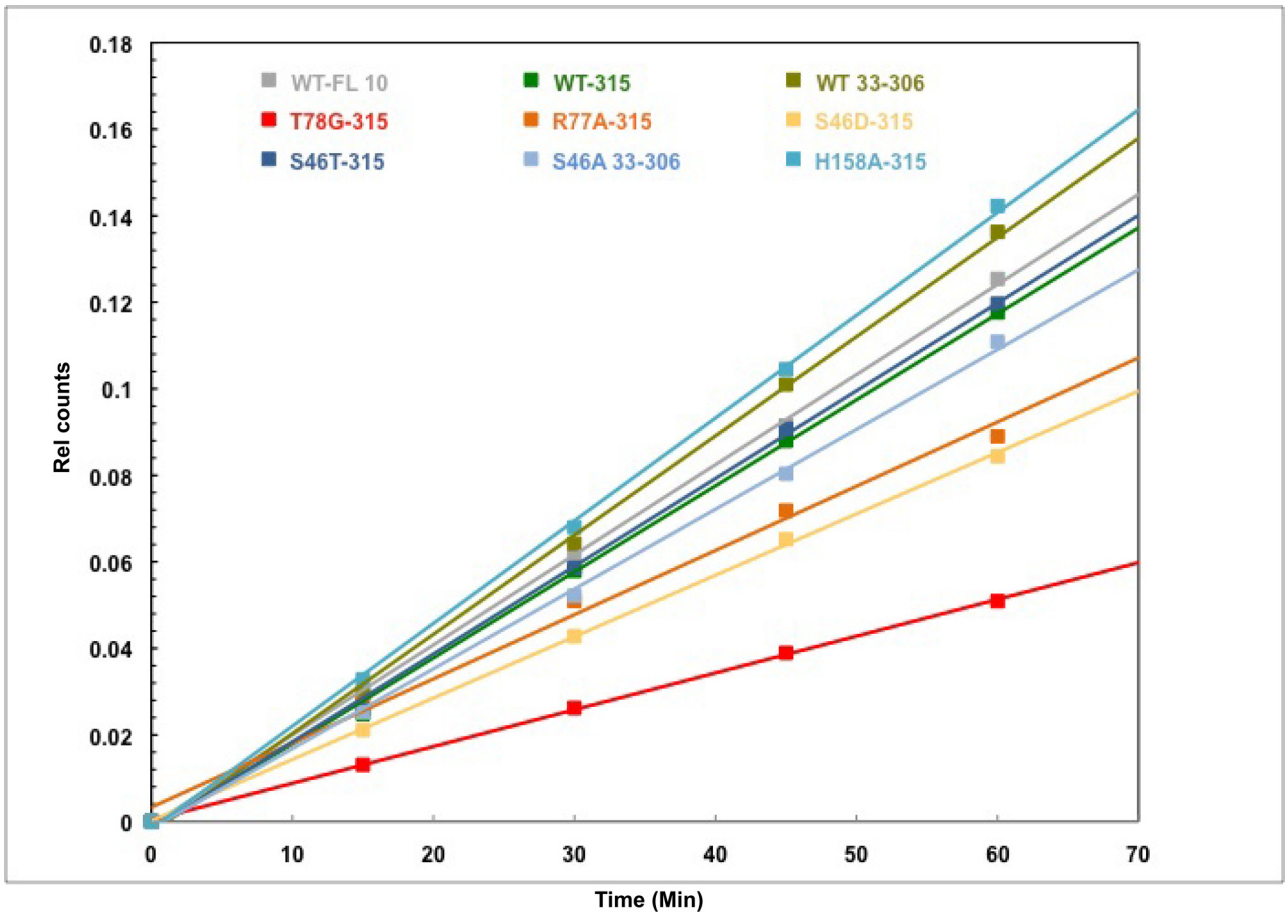

Fig. S5. GTPase assay of SEPT2 mutants.

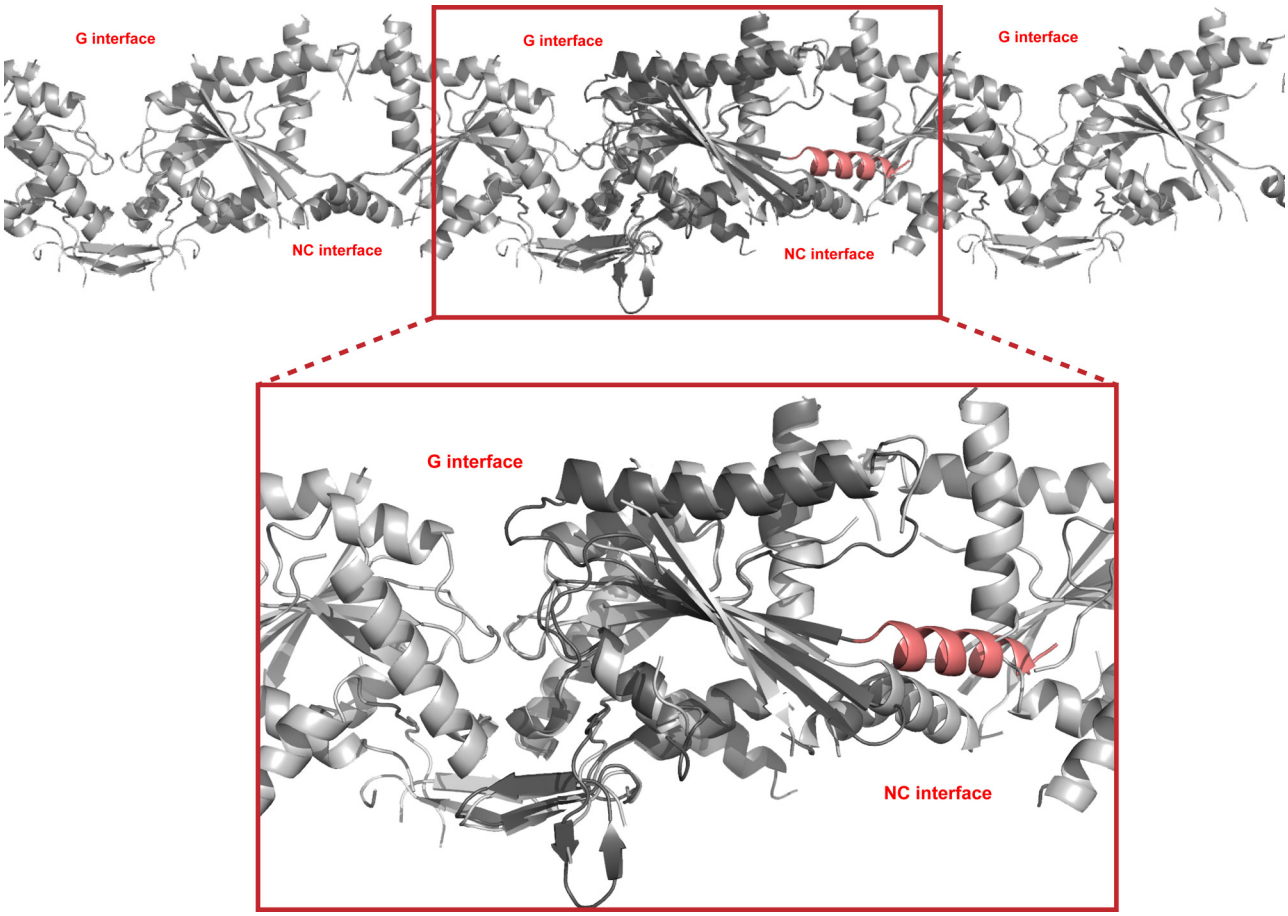

Fig. S6. SEPT2-ΔN-GppNHp (dark gray) overlaid on a septin filament model (light gray) generated using the 2QA5 model. The N-terminal helix, α0 (red), was modeled in SEPT2-ΔN-GppNHp. The α0 in GTP-bound form causes steric interference with the neighboring subunit, thereby destabilizing the NC interface.

Table S1. Crystallographic table of SEPT2-ΔN

Wavelength, Å	0.9790
Space group	P212121
Cell dimensions	65.98, 118.44, 190.82
Resolution, Å*	20–2.9 (3.0–2.9)
Rsym, (%)*,†	6 (37.2)
I / σ I (I)*	20.07 (4.81)
Completeness (%)*	99.3 (99.8)
Redundancy	4.8
Number of reflections	32,071
R_{work}‡/R_{free}§	24.8/29.0
Total number of atoms	8,385
Protein atoms	8,150
Ligand/ion atoms	132
Water atoms	103
B-factors	
Protein	42.8
Ligand/ion	30.5
Water	47.2
RMS deviations	
Bond lengths, Å	0.009
Bond angles, degrees	1.224
PDB ID	3FTQ

*Values in the parentheses indicate outermost shells.

†$R_{sym} = \Sigma|Ih–<Ih>| / \Sigma ih$, where $<Ih>$ is the intensity of the symmetry-equilvalent measurements.

‡$R_{work} = \Sigma|FO - FC| / \Sigma FO$, where *FO* and *FC* are the observed and calculated structure factor amplitudes.

§R_{free} is calculated similarly to R_{work} using the test set reflections.

Table S2. GDP and GTP affinity constants of SEPT2 WT and mutants

Protein	GDP, μM	GTP (GppNHp), μM
WT–315	3.75	3.96
WT 33–306	5.4	4.7
T78G–315	3.6	$\approx$ 75
R77G–315	7.6	2.7
S46A 33–306	2	9.8
S46D–315	$\approx$36	ND*
S46T–315	1	3.75

*No fluorescent change detected during assay.

Table S3. Yeast strains and plasmids

Strain/plasmid	Description	Source
BY4743	*MATa/α his3Δ1/ his3Δ1 leu2Δ0/leu2Δ0 met15Δ0/MET15 lys2Δ0/LYS2 ura3Δ0/ura3Δ0*	EUROSCARF
Y25223	BY4743 *cdc3*::*KANMX4/CDC3*	EUROSCARF
Y22554	BY4743 *cdc11*::*KANMX4/CDC11*	EUROSCARF
Y21935	BY4743 *cdc12*::*KANMX4/CDC12*	EUROSCARF
FMY1086	*MATα his3Δ1 leu2Δ0 met15Δ0 LYS2 ura3Δ0 cdc3*::*KANMX4* pFM337	This study
FMY1089	*MATα his3Δ1 leu2Δ0 MET15 LYS2 ura3Δ0 cdc11*::*KANMX4* pFM581	This study
FMY1092	*MATα his3Δ1 leu2Δ0 met15Δ0 lys2Δ0 ura3Δ0 cdc12*::*KANMX4* pFM338	This study
pRS415	*CEN, LEU2*	(42)
pRS416	*CEN, URA3*	(42)
pFM337	pRS416 *CDC3*	This study
pFM338	pRS416 *CDC12*	This study
pFM580	pRS416 *CDC10*	This study
pFM581	pRS416 *CDC11*	This study
pFM582	pRS315 *cdc3H262A*	This study
pFM650	pRS415 *CDC12*	This study
pFM651	pRS415 *cdc12H155A*	This study
pFM653	pRS415 *CDC11*	This study
pFM654	pRS415 *cdc11H147A*	This study
pFM656	pRS415 *CDC10*	This study
pFM657	pRS415 *cdc10K155A*	This study
pFM820	pRS415 *cdc3D128A*	This study
pFM821	pRS415 *cdc3D128S*	This study
pFM823	pRS415 *cdc10S41A*	This study
pFM824	pRS415 *cdc10T74A*	This study
pFM826	pRS415 *cdc11S31A*	This study
pFM828	pRS415 *cdc12S43A*	This study
pFM829	pRS415 *cdc12T75A*	This study
pFM831	pRS415 *CDC3*	This study
pFM842	pRS415 *cdc3D210A*	This study
pFM843	pRS415 *cdc10D103A*	This study